

Electric field inside a “Rosky cavity” in uniformly polarized water

Daniel R. Martin,¹ Allan D. Friesen,¹ and Dmitry V. Matyushov^{1, a)}

Center for Biological Physics, Arizona State University, PO Box 871604, Tempe, AZ 85287-1604

(Dated: 2 June 2019)

Electric field produced inside a solute by a uniformly polarized liquid is strongly affected by dipolar polarization of the liquid at the interface. We show, by numerical simulations, that the electric “cavity” field inside a hydrated non-polar solute does not follow the predictions of standard Maxwell’s electrostatics of dielectrics. Instead, the field inside the solute tends, with increasing solute size, to the limit predicted by the Lorentz virtual cavity. The standard paradigm fails because of its reliance on the surface charge density at the dielectric interface determined by the boundary conditions of the Maxwell dielectric. The interface of a polar liquid instead carries a preferential in-plane orientation of the surface dipoles thus producing virtually no surface charge. The resulting boundary conditions for electrostatic problems differ from the traditional recipes, affecting the microscopic and macroscopic fields based on them. We show that relatively small differences in cavity fields propagate into significant differences in the dielectric constant of an ideal mixture. The slope of the dielectric increment of the mixture versus the solute concentration depends strongly on which polarization scenario at the interface is realized. A much steeper slope found in case of Lorentz polarization also implies a higher free energy penalty for polarizing such mixtures.

Keywords: Cavity field, surface polarization, hydration, polar response.

I. INTRODUCTION

When an interface is created in a dielectric, the surface dipoles change their preferential orientations relative to the dipoles in the bulk. The response of the dielectric to a weak external field is then a composite result of the response of these surface dipoles and the bulk dipoles. The question of whether the dielectric response of a material is sensitive to its surface structure is decided by the relative weights of these two contributions.

The Maxwell electrostatics of dielectrics neglects the structure of the interface and replaces the interfacial region of a finite microscopic dimension with an infinitesimally thin mathematical surface. This mathematical surface cuts through the dipoles of the medium creating a surface charge with the charge density σ_P (Fig. 1a). It is given by the projection of the dipolar polarization at the interface $\mathbf{P}(\mathbf{r}_S)$ on the outward normal $\hat{\mathbf{n}}$ to the surface bounding the dielectric,¹ $\sigma_P(\mathbf{r}_S) = P_n(\mathbf{r}_S)$, $P_n(\mathbf{r}_S) = \hat{\mathbf{n}} \cdot \mathbf{P}(\mathbf{r}_S)$.

The surface charge density produces the electric field of its own, which polarizes the dielectric to form an inhomogeneous polarization $\mathbf{P}(\mathbf{r})$ near the interface. It decays to the uniform polarization field \mathbf{P} , associated with a uniform external field \mathbf{E}_{ext} , far from the interface. Since the spatial extent of the interface is neglected, the polarization $\mathbf{P}(\mathbf{r})$ extends continuously up to the mathematical dividing surface. If the dielectric borders vacuum, the polarization field changes discontinuously from $\mathbf{P}(\mathbf{r}_S)$ at the dielectric side of the surface to zero at its vacuum side.

The sum of the electric field from the surface charge

density and the external field is the Maxwell field $\mathbf{E}(\mathbf{r})$. The Maxwell field, as well as the polarization $\mathbf{P}(\mathbf{r})$, cannot be directly measured, but can be retrieved from electric fields inside cavities carved in the dielectric, as originally suggested by Thompson and Maxwell.^{2,3} For the simplest geometry of an empty spherical cavity, the solution of the Laplace equation with Maxwell’s boundary conditions gives the field at the cavity center (cavity field)^{1,4}

$$E_M = \frac{3}{2\epsilon + 1} E_{\text{ext}}, \quad (1)$$

where ϵ is the dielectric constant of the medium surrounding the cavity. The qualitative prediction of this result is that external field E_{ext} is diminished by a factor of $3/(2\epsilon)$ inside cavities created in highly polar dielectrics such as water. This scenario then describes a well-defined physical setup testable by laboratory or numerical experiment.

One wonders to what extent the mathematical formalism of Maxwell’s electrostatics applies to interfaces of polar liquids. The interface is obviously not a mathematical surface, but has a finite width (Laplace vs Poisson definition of the interface⁵). In addition, liquid dipoles have the freedom to rotate and adjust to the lack of molecular interactions from the cavity side of the interface. For polar liquids, this restructuring results in preferential in-plane orientation of the liquid dipoles at free planar and closed interfaces.^{6–12} Unless the external field orients the dipoles off-plane, such orientational structure eliminates the surface charge since $\sigma_P = P_n \simeq 0$ (Fig. 1b). The standard boundary conditions of Maxwell’s electrostatics do not apply, thus affecting the observable cavity field.

Water presents a particularly important test case for understanding the interfacial electrostatics of polar liquids. Strong hydrogen bonds between surface waters can

^{a)}Electronic mail: dmitrym@asu.edu

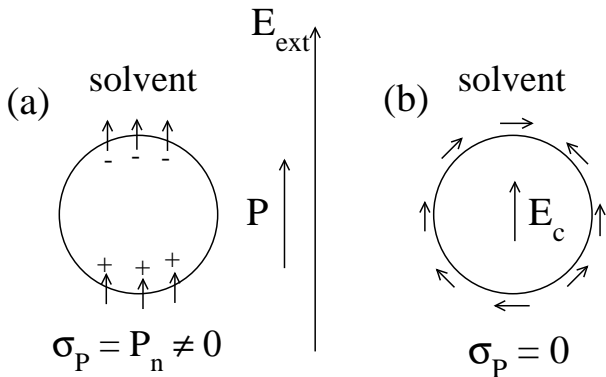


FIG. 1. Cartoon of the charge distribution σ_P at the surface of a spherical cavity carved from a liquid dielectric. Panel (a) represents the picture of standard Maxwell’s electrostatics of dielectrics, when the normal projection of the dipolar polarization \mathbf{P} along the external field \mathbf{E}_{ext} creates the positive and negative lobes of the surface charge distribution. Those result from the mathematical surface cutting through polarized dipoles of the liquid shown by arrows. The overall electric field inside the cavity is then reduced from the external field by the opposing field of the surface charges [Eq. (1)]. Panel (b) shows the scenario suggested by the orientational dipolar order at the surface of a “Rosicky cavity” in a polar liquid.^{6–12} In-plane orientations of the surface dipoles, unaltered by a weak external field, do not produce surface charge. The result is zero surface charge density σ_P and the field at the cavity center following the Lorentz equation [Eq. (2)]. Both sets of lines have been produced with $\epsilon = 72.2$ for SPC/E water at 300 K.

potentially prevent their reorientation not only by a weak external field of the dielectric experiment, but also by internal fields of solute charges. Since it is the response of the water dipoles that determines the free energy of hydration,¹³ this problem goes beyond the question of measuring the electric field inside a dielectric cavity in Maxwell’s “gedanken experiment”.

We have previously approached the problem of liquid interfacial electrostatics by literally following Maxwell’s recipe and measuring, by numerical simulations, the electric field inside an empty hard-sphere cavity carved in the model fluid of dipolar hard spheres.^{14,15} These studies have shown that the cavity field indeed does not continuously decrease with increasing ϵ , as Eq. (1) would suggest, but instead levels off, as a function of ϵ , at a value close to the result well established in the theory of dielectrics. This limit corresponds to the Lorentz virtual cavity.⁴ The latter is defined as a part of the dielectric confined by a mathematical closed surface inside it. The Lorentz cavity field is then the field produced by the dielectric outside this surface. Since no physical interface is present, there is no physical polarization at the interface and $\sigma_P = 0$ by definition.¹⁶

The electric field at the center of a virtual cavity is obtained by integrating over the field contributions from homogeneous polarization of the medium, instead of in-

homogeneous polarization in the case of Maxwell’s electrostatics (see below). The field accumulated by this uniform polarization results in the Lorentz field at the cavity center

$$E_L = \frac{\epsilon + 2}{3\epsilon} E_{\text{ext}}. \quad (2)$$

The main qualitative difference between this result and the standard cavity field given by Eq. (1) is that the Lorentz field does not decay to zero at $\epsilon \rightarrow \infty$ and instead levels off at a non-zero value of $E_L/E_{\text{ext}} \rightarrow 1/3$.

The model dipolar system studied previously by us^{14,15} has in principle shown that interfacial orientational structure of a polar liquid might be closer to the limiting scenario sketched in Fig. 1b than to the standard, solid-like picture sketched in Fig. 1a. The question of practicality of this observation remains however open. A vacuum hard-sphere cavity is a purely theoretical construct. Nevertheless, the scenario arising from this model can potentially describe non-polar particles solvated in real polar liquids.

In order to approach this more realistic situation, we study here the scenario that we have dubbed the “Rosicky cavity”. The actual system is a Lennard-Jones (LJ) solute inserted in SPC/E water. As was originally shown by Rosicky and co-workers⁶ and supported by many subsequent studies,^{7–12} water dipoles orient in-plane at interfaces with non-polar solutes. Although a non-polar solute studied here is certainly not a cavity, the orientational water structure is highly resilient to external perturbations and remains nearly intact for a broad range of solute-solvent attractions.¹⁷ The term “cavity” is then used to stress that it is a large energy of the water hydrogen bonds ($\Delta H \simeq 4 - 5 k_B T$ per bond for SPC/E water¹⁸) that supports the interfacial orientational structure. Therefore, in contrast to the virtual Lorentz cavity, this physical cavity, like the traditional Maxwell cavity, is meant to represent realistic measurements of local fields inside dielectrics, in water in the present study. The Rosicky cavity is meant to represent physical situations when the interfacial structure is dominated by in-plane orientations of water dipoles. We show that the boundary conditions imposed by molecular interfacial order of this cavity produce the electrostatic response approaching the conditions expected for the virtual Lorentz cavity and thus dramatically deviating from the Maxwell cavity field.

II. RESULTS

The model considered here consists of a single non-polar solute interacting with a large number of waters mimicking a typical solvation experiment. The solute-water interaction is modeled by a Kihara potential combining a hard-sphere core of the radius R_{HS} with a surface

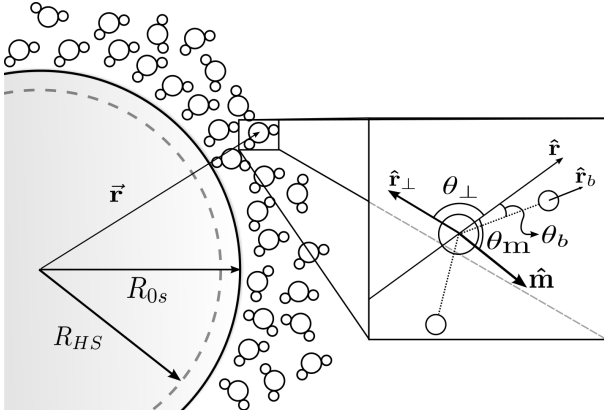


FIG. 2. A cartoon of the Kihara solute in SPC/E water and the definition of the projection angles describing the orientations of waters in the first hydration layer in respect to the surface normal $\hat{\mathbf{n}} = -\hat{\mathbf{r}}$. θ_b is the angle between O-H bond and $\hat{\mathbf{r}}$, θ_m is the angle between the water dipole and $\hat{\mathbf{r}}$, θ_\perp defines the orientation of the plane of H₂O (note that $\hat{\mathbf{m}} \cdot \hat{\mathbf{r}}_\perp = 0$).

LJ layer of width σ_{0s} (Fig. 2)

$$\phi_{0s}(r) = 4\epsilon_{0s} \left[\left(\frac{\sigma_{0s}}{r - R_{HS}} \right)^{12} - \left(\frac{\sigma_{0s}}{r - R_{HS}} \right)^6 \right]. \quad (3)$$

Here, “0” and “s” are used to label the solute and solvent (water), respectively; ϵ_{0s} is the energy of solute-solvent LJ attraction. Further, in order to map hard-sphere cavities used in our previous studies^{14,15} on the “soft” Kihara solute, we adopt the radius of the closest approach

$$R_{0s} = R_{HS} + \sigma_{0s}, \quad (4)$$

where $\sigma_{0s} = 3.0 \text{ \AA}$ has been used in all numerical calculations.

The Kihara potential is the only solute-solvent interaction introduced in our present model. We are therefore missing the effect of electronic polarizability of the solute always present even for non-polar particles. A crude way to estimate this effect is to notice that only the ratio of the dielectric constants of two interfacing media matters for the interfacial dielectric response in dielectric theories.¹ While this prescription requires testing for microscopic liquid interfaces, the model situation of a fully non-polarizable solute can be mapped on real situations of solvated non-polar particles by rescaling the solvent dielectric constant with the dielectric constant ϵ_0 of the solute, $\epsilon \rightarrow \epsilon/\epsilon_0$, if such property can be reasonably defined. We will therefore proceed with the present model using the term “cavity field” to describe the electric field at the center of the solute.

Configurations of the water-solute mixture were produced by Molecular Dynamics (MD) simulations of a single solute inserted in a box of SPC/E waters at standard conditions (Supplementary Material (SM)¹⁹). The ratio of the cavity and external fields is obtained in the linear response approximation as the correlator of the electric

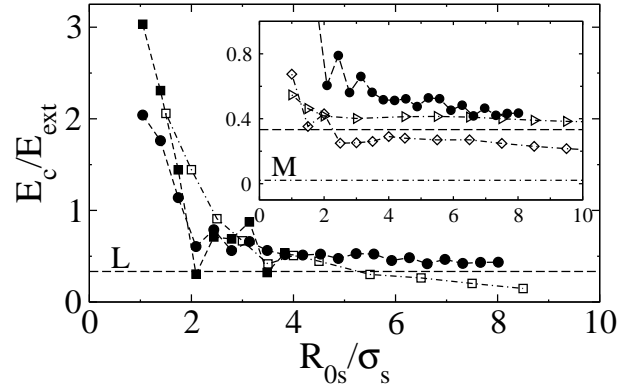


FIG. 3. The cavity field inside Kihara solutes (filled points, connected by the dashed lines) compared to hard-sphere cavities inside dipolar fluids (open points, connected by the dash-dotted lines).¹⁴ Results of MD simulations in the main panel refer to two values of the solute-solvent LJ attraction, $\epsilon_{0s} = 0.65 \text{ kJ/mol}$ (circles) and 20.0 kJ/mol (squares). The results for the Kihara solutes are plotted against the radius of closest approach R_{0s}/σ_s defined by Eq. (4) ($\sigma_s = 2.87 \text{ \AA}$). Open points in the main panel and the inset refer to sets of data obtained for varied reduced dipole moment $(m^*)^2 = \beta m^2/\sigma_s^3$ of the dipolar hard-sphere fluids: 0.5 (diamonds), 1.0 (triangles), and 3.0 (squares). The results for hard-sphere cavities in dipolar fluids are plotted against the radius of the closest hard-sphere solute-solvent approach R_{0s}/σ_s ; σ_s is the diameter of the solvent hard spheres. The dashed horizontal lines in the main panel and in the inset refer to the Lorentz result (L) of Eq. (2). The dash-dotted horizontal line in the inset refers to the Maxwell result (M) of Eq. (1).

field \mathbf{E}_s produced by water at the solute center with the water dipole moment \mathbf{M}_s

$$E_c/E_{\text{ext}} = 1 + (\beta/3)\langle \delta\mathbf{E}_s \cdot \delta\mathbf{M}_s \rangle - E_{\text{corr}}. \quad (5)$$

Here, $\delta\mathbf{E}_s$ and $\delta\mathbf{M}_s$ denote deviations from the corresponding average values and $\beta = 1/(k_B T)$ is the inverse temperature. In addition, the correction term E_{corr} in the rhs of Eq. (5) accounts for the cutoff of the electrostatic interactions specific to a given simulation protocol. The result for Ewald sums is given in the SM,¹⁹ while the reaction field protocol was covered in previous studies.^{14,15}

Equation (5) was used to calculate the field inside the solutes of varying size R_{HS} of the Kihara hard-sphere core, and the results are plotted in Fig. 3. In order to assess the effect of a uniform solute-solvent attraction on the cavity field we have simulated the configurations at two values of the LJ attraction, $\epsilon_{0s} = 0.65 \text{ kJ/mol}$ equal to the LJ energy between oxygens of SPC/E water and $\epsilon_{0s} = 20 \text{ kJ/mol}$ close to the energy required to break two hydrogen bonds in bulk SPC/E water.¹⁸

The smaller value of the LJ attraction perturbs little the water structure at small values of R_{HS} , but results in a weakly dewetted interface²⁰ at the end of the scale of R_{HS} values. This is meant to imply that the first peak of the solute-solvent radial distribution function falls below

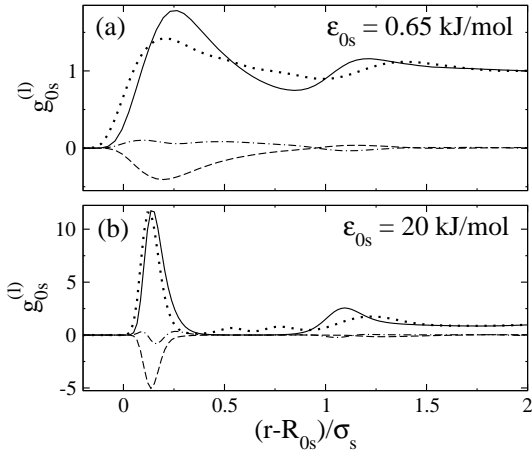


FIG. 4. The solute-solvent distribution functions $g_{0s}^{(\ell)}(r)$ [Eq. (6)] vs the distance from the surface of the Kihara solute ($R_{0s} = 13$ Å). Shown are the solute-oxygen (solid lines) and solute-hydrogen (dotted lines) radial distribution functions ($\ell = 0$) and orientational distributions for $\ell = 1$ (dash-dotted lines) and $\ell = 2$ (dashed lines); (a) refers to $\epsilon_{0s} = 0.65$ kJ/mol and (b) refers to $\epsilon_{0s} = 20.0$ kJ/mol.

the corresponding peak of the solvent-solvent distribution function. On the contrary, the larger value of the solute-solvent LJ attraction produced a substantial increase of the surface density of water as judged from the solute-solvent pair distribution function (Fig. 4). Furthermore, the radial distribution function is nearly zero between the first and second hydration shells indicating layering of water at the interface.²¹

In order to characterize the orientational structure of the interfacial water dipoles, we define a series of distribution functions recognizing the radial symmetry of the problem and producing increasing symmetry orders of the water dipoles $\hat{\mathbf{m}}_j$ in projection on the outward normal to the spherical solute surface $\hat{\mathbf{r}}_j$ at the position \mathbf{r}_j of a water molecule (oxygen coordinates are used for the center of mass). The radial distribution functions are then defined in terms of ℓ -order Legendre polynomials $P_\ell(\cos \theta_{mj})$, $\cos \theta_{mj} = \hat{\mathbf{m}}_j \cdot \hat{\mathbf{r}}_j$ as follows

$$g_{0s}^{(\ell)}(r) = (V/N) \sum_j P_\ell(\cos \theta_{mj}) \delta(\mathbf{r}_j - \mathbf{r}). \quad (6)$$

Here, V and N are the system volume and the number of particles, respectively. The zeroth-order distribution function is then the standard solute-oxygen radial distribution $g_{0s}^{(0)}(r) = g_{0s}(r)$. In addition to these radial distributions shown in Fig. 4, we also calculate the order parameters of the dipoles in the first hydration layer by integrating the radial functions over the volume V^I defined by the condition $0 < r < R_{0s} + \sigma_s/2$

$$p_\ell^I = (N^I)^{-1} \rho_s \int_{V^I} g_{0s}^{(\ell)}(r) d\mathbf{r}. \quad (7)$$

Here, ρ_s is the water number density and the integrated radial function is normalized to the number of waters in

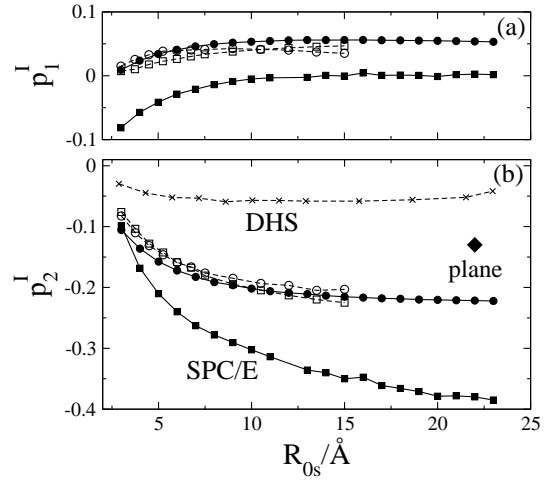


FIG. 5. The first (upper panel) and second (lower panel) orientational order parameters $p_{1,2}^I$ of the first-shell SPC/E waters vs $R_{0s} = R_{HS} + \sigma_{0s}$. The solid circles ($\epsilon_{0s} = 0.65$ kJ/mol) and squares ($\epsilon_{0s} = 20$ kJ/mol) refer to Kihara solutes in water at $T = 300$ K. The corresponding open points refer to $T = 273$ K. The crosses in the lower panel show p_2^I for HS cavities in the fluid of dipolar hard spheres (DHS)²² with the reduced dipole moment $(m^*)^2 = \beta m^2 / \sigma_s^3 = 3.0$; m is the dipole moment and σ_s is the HS diameter of the solvent. The filled diamond labeled “plane” marks p_2^I for a planar water interface from Ref. 9.

the first hydration layer

$$N^I = \rho_s \int_{V^I} g_{0s}^{(0)}(r) d\mathbf{r}. \quad (8)$$

The results for first-order, p_1^I , and second-order, p_2^I , order parameters vs the solute size are plotted in Fig. 5.

The structure of surface waters is a “squashed” hexagonal ice lattice in which two oxygen sublayers of hexagonal sheets are brought into one plane of the closest solute-solvent approach corresponding to the first peak of the solute-oxygen radial distribution function (Fig. 4). The hydrogens of first-shell waters are randomly distributed for weak solute-solvent attraction of a hydrophobic surface⁶ (Fig. 4a), but get ordered with increasing the attractive pull of the solute (Fig. 4b). The breaking of the sublayers of the hexagonal ice sheets results in buckling of the O–H–O bond²³ from the straight line found in hexagonal ice to preferential angles of $\sim 10^\circ$ (more populated) and $\sim 70^\circ$ (less populated) (see the SM¹⁹). This distribution of hydrogen-bond angles is also quite insensitive to the strength of the LJ attraction. Further, consistent with a broad distribution of the first-shell hydrogens shown by the dotted lines in Fig. 4, the water dipoles are broadly distributed for weak solute-solvent attraction, but become more ordered when LJ attraction becomes stronger (Fig. 6b). In all cases, however, the in-plane orientation of the water dipoles is preferred, and is highly resilient to the changes in the solute-solvent attraction.

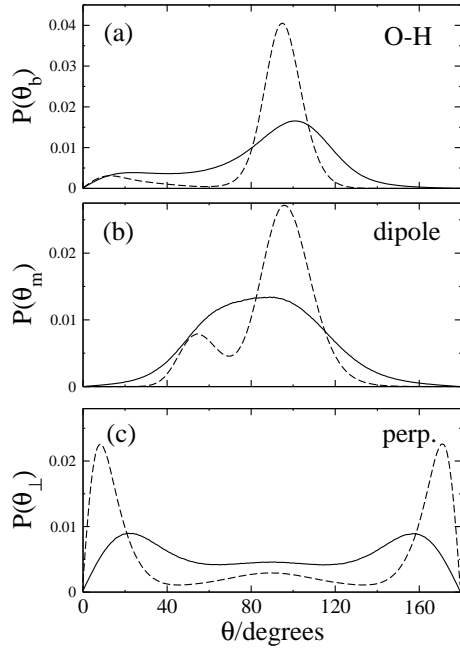


FIG. 6. Distributions of three angles used to define the water orientations relative to the radial direction (Fig. 2): (a) θ_b for the O–H bond ($\cos \theta_b = \hat{r}_b \cdot \hat{r}$), (b) θ_m for the water dipole ($\cos \theta_m = \hat{m} \cdot \hat{r}$), and (c) θ_\perp for the normal to H_2O plane ($\cos \theta_\perp = \hat{r}_\perp \cdot \hat{r}$); $R_{0s} = 13 \text{ \AA}$.

The distributions of projections of water O–H bonds and the normal to the H_2O plane (Fig. 2) are shown in Fig. 6a,c. Both are consistent with the picture of the in-plane orientation of the water dipoles, with the first-shell waters populating variably the states of H_2O plane perpendicular to the surface normal and slightly tilted, at $\sim 10^\circ$ in respect to the normal. These two states are populated in the ratio of about 1:2 for the weak attraction, but the tilted state becomes a dominant one at the stronger attraction. This observation is consistent with the general tendency of interfacial waters to increasingly occupy one particular orientational state with increasing strength of attraction of either protons or oxygens to the solute. In contrast, the hydrogen disorder generally increases when a combination of two types of attractions are present at the interface,²⁴ a situation typical of hydrated proteins.

III. DISCUSSION

The results for the electric field inside the Rossky cavity in water are shown by filled points in Fig. 3. They clearly tend to the Lorentz field limit. We also plot in Fig. 3 (open points) the results for the electric field inside hard-sphere cavities in dipolar fluids.^{14,15} Although the two situations are physically distinct, a non-polar solute in the former case vs an actual cavity in the latter, the phenomenology of the polar interfacial response is generic

for both cases. The common output of these two sets of simulations suggests that the picture of non-polarized interface represents the response of free and non-polar interfaces of polar liquids in general.

It is instructive to see how the Maxwell cavity field and the Lorentz field appear based on the assumptions regarding the surface charge density (Fig. 1a,b). We first assume a constant value for the surface charge density $\sigma_P = \sigma_0$. The Maxwell electric field in the medium is then the sum of the external field and the radial field propagating from a uniformly charged interface

$$\mathbf{E}(\mathbf{r}) = \frac{1}{\epsilon} \mathbf{E}_{\text{ext}} + \frac{4\pi R_0^2 \sigma_0}{\epsilon r^3} \mathbf{r}. \quad (9)$$

This electric field will polarize the dielectric yielding the polarization field $\mathbf{P}(\mathbf{r}) = (\epsilon - 1)\mathbf{E}(\mathbf{r})/(4\pi)$. This polarization field is inhomogeneous close to the interface and decays to the uniform polarization \mathbf{P} in the bulk. The polarization of the dielectric will in turn produce its own electric field, which, combined with the external field, gives the cavity field

$$\mathbf{E}_c = \mathbf{E}_{\text{ext}} + \int_{\Omega} \mathbf{T}(\mathbf{r}) \cdot \mathbf{P}(\mathbf{r}) d\mathbf{r}. \quad (10)$$

Here, $\mathbf{T}(\mathbf{r}) = \nabla \nabla r^{-1}$ is the dipolar interaction tensor and the integral is over the dielectric occupying the volume Ω outside the dielectric cavity of radius R_0 . The radius R_0 does not need to be specified since the calculation results do not depend on its value.

The radial polarization arising from the second summand in Eq. (9) gives zero contribution to the cavity field and the result of Eqs. (9) and (10) is the Lorentz field given by Eq. (2). A constant, angular-independent surface charge density makes therefore no contribution to the cavity field. It however contributes to a non-zero, spatially constant electrostatic potential inside the cavity.²⁵

Given axial symmetry of the problem, surface charge density can be expanded in Legendre polynomials, $\sigma_P(\theta) = \sum_{\ell} \sigma_{\ell} P_{\ell}(\cos \theta)$, where θ is the polar angle with the direction of the external field. Since the zero-order term σ_0 does not contribute to the cavity field, one can take the first-order term and, neglecting the quadrupolar and higher moments, have the dipolar approximation $\sigma_P(\theta) = \sigma_1 \cos \theta$. The dipole moment created by the solute interface is then $M_0 = \sigma_1 \Omega_0$. This is the situation sketched in Fig. 1a. The direct solution of the Laplace equation with Maxwell's boundary conditions results in the interfacial dipole

$$\mathbf{M}_0 = -\mathbf{P} \frac{3\Omega_0}{2\epsilon + 1}, \quad (11)$$

where $\mathbf{P} = (\epsilon - 1)/(4\pi\epsilon)\mathbf{E}_{\text{ext}}$. The negative sign here indicates that the interface dipole \mathbf{M}_0 orients oppositely to the external field, as is also clear from Fig. 1a.

The dipolar surface charge density following from Eq. (11) is shown by the solid line in Fig. 7. This surface

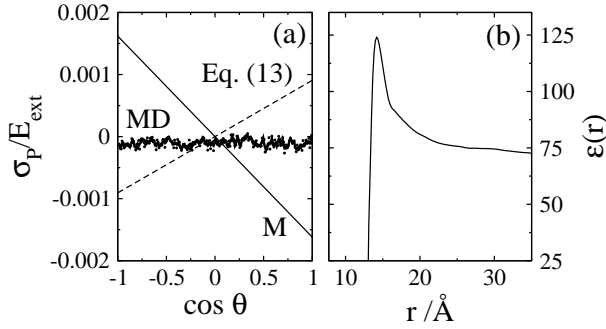


FIG. 7. Surface charge density $\sigma_P(\theta) = P_n(\theta)$ vs the polar angle θ measured from the direction of the external field (a). The solid line (M) shows the result of Maxwell’s electrostatics [Eq. (16), $\epsilon = 72.2$ for SPC/E water at 300 K]. The dots refer to σ_P calculated as a linear response to an external field from 40 ns of MD trajectories (see the SM¹⁹). The MD σ_P is collected from a water layer $R_{0s} \leq r \leq R_{0s} + 0.1\sigma_s$ for the solute with the size $R_{0s} = 13 \text{ \AA}$ and $\epsilon_{0s} = 0.65 \text{ kJ/mol}$. The dashed line shows the result of using E_c from simulations to calculate χ_1 from Eq. (13). Panel (b) shows the profile of water’s dielectric constant $\epsilon(r) = 1 + (4\pi\beta/3\Omega(r))\langle\delta\mathbf{M}_s(r) \cdot \delta\mathbf{M}_s\rangle$ (see text).

charge density creates a dipolar field, which adds to the external field to produce the Maxwell field

$$\mathbf{E}(\mathbf{r}) = \frac{1}{\epsilon}\mathbf{E}_{\text{ext}} + \mathbf{T}(\mathbf{r}) \cdot \mathbf{M}_0. \quad (12)$$

When the polarization field $\mathbf{P}(\mathbf{r})$ is calculated from Eq. (12) and substituted into Eq. (10), the cavity field becomes

$$\frac{E_c}{E_{\text{ext}}} = \frac{\epsilon + 2}{3\epsilon} + \frac{8\pi(\epsilon - 1)}{9}\chi_1, \quad (13)$$

where

$$\chi_1 = \frac{M_0}{\Omega_0 E_{\text{ext}}} \quad (14)$$

is the dipolar response function of the solute interface to the polarizing external field. The Maxwell result for M_0 in Eq. (11) gives the standard cavity field of Eq. (1), while $\chi_1 = M_0 = 0$ leads to the Lorentz field of Eq. (2).

Surface charge density $\sigma_P(\theta)$ provides a convenient mathematical idealization of the polarization of the interface. Its direct calculation from real-space, finite-size simulations presents, however, a significant challenge. The problem is illustrated in Fig. 7a which shows $\sigma_P(\theta)$ calculated at the solute surface from MD trajectories using the linear response approximation (see the SM¹⁹). The result is a clearly angular-independent function, producing $\sigma_1 \simeq 0$ and $E_c \simeq E_L$. This outcome is, however, not entirely consistent with a slightly positive σ_1 following from the substitution of the simulated E_c into Eq. (13) (dashed line in Fig. 7a).

The reason of possible uncertainties in the attempts to calculate $\sigma_P(\theta)$ from sampling surface dipole directions from MD trajectories is illustrated in Fig. 7b. The

definition of a mathematical dividing surface is uncertain when the dipolar response is strongly varied at the interface, as is the case here. We show the dielectric constant of the polar layer of radius r from the cavity center obtained from the linear response approximation as²⁶ $\epsilon(r) = 1 + (4\pi\beta/3\Omega(r))\langle\delta\mathbf{M}_s(r) \cdot \delta\mathbf{M}_s\rangle$, where $\mathbf{M}_s(r)$ and $\Omega(r)$ are, respectively, the dipole moment and volume of the solvent within the r -surface. The layer dielectric constant peaks near the interface and then slowly decays to the bulk dielectric constant ϵ . Any surface drawn next to the interface will therefore reflect a different variance of the surface dipole, with a different outcome for $\sigma_P(\theta)$. How much the functional form of $\sigma_P(\theta)$ changes depending on the surface definition cannot be answered here. Attempts to obtain $\sigma_P(\theta)$ at surfaces deeper into the bulk did not produce converged functions and therefore are not shown here.

It seems worth emphasizing some critical differences between both (Maxwell and Lorentz) continuum results and the molecular picture offered by the present numerical simulations. The continuum cavity field does not depend on the cavity size, but only on the cavity shape (e.g., on the length/diameter ratio for a cylindrical cavity^{3,4}). This is of course the consequence of neglecting the actual spread of the interfacial region relative to the size of the solute, which is behind the definition of the interface as a mathematical dividing surface. Our simulations allow us to estimate the solute size at which this approximation becomes valid. Figure 3 shows that the cavity field starts leveling off to a size-independent limit at $R_{0s}/\sigma_s \simeq 2 - 2.5$. It gives an estimate of the solute size at which the “Lorentz continuum” starts to take hold: the solute needs to be 4 – 5 times larger than the solvent molecule. The “Maxwell continuum” is, however, never reached in our simulations.

IV. EXPERIMENTAL OBSERVABLES

The surface polarization effects discussed here have a number of consequences observable in a macroscopic laboratory experiment. The total free energy of polarizing the dielectric is measured by the dielectric experiment and is affected by the dipole accumulated at the interface with a non-polar solute. The total dipole of a mixture sample M_{mix} is reduced relative to the homogeneous solvent by the volume excluded by the solute and, in addition, is affected by the dipole of the interface

$$\mathbf{M}_{\text{mix}} = \mathbf{P}\Omega - (2/3)(\epsilon - 1)\mathbf{M}_0 N_0. \quad (15)$$

Here, N_0 is the number of the solutes in the solution and Ω , as above, is the solvent volume. The solutes are assumed to be non-interacting, although the theory can be extended to non-ideal solutions requiring the solute-solute structure factor as an additional input.²⁷

The standard arguments of the theory of dielectrics then suggest the equation for the dielectric constant of

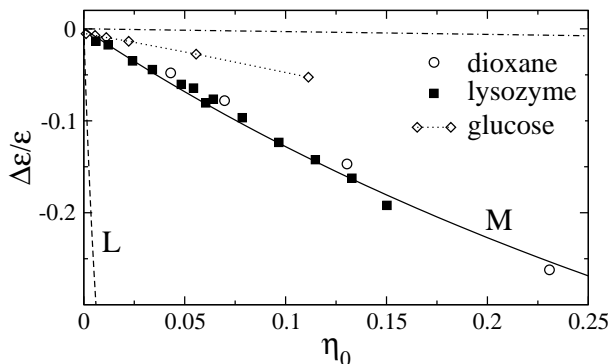


FIG. 8. Relative dielectric constant increment $\Delta\epsilon/\epsilon$, $\Delta\epsilon = \epsilon_{\text{mix}} - \epsilon$ for several aqueous solutions: lysozyme²⁹ (filled squares), dioxane³⁰ (open circles), glucose³¹ (open diamonds), and trehalose³² (dash-dotted line). The solid line (M) shows the result of Eq. (18), while the dashed line (L) is the dielectric increment for a solute with no surface charge density, $\sigma_1 = 0$, and therefore Lorentz result for the cavity field [Eq. (13)]. Experimental and calculation results used to convert the experimentally reported solute concentrations to volume fractions can be found in the SM.¹⁹

the mixture^{15,27}

$$\frac{\epsilon}{\epsilon_{\text{mix}}} = 1 + \eta_0(\epsilon - 1)(1 + (8\pi/3)\epsilon\chi_1), \quad (16)$$

where $\eta_0 = N_0\Omega_0/(N_0\Omega_0 + \Omega)$ is the volume fraction of the solutes. Equations (13) and (16), taken together, suggest that dielectric constants of low-concentration solutions and cavity fields inside solutes both give experimental routes to measure the dipolar response function of the interface χ_1 .

For the interface dipole given by Maxwell's form in Eq. (11),

$$\chi_1 = -\frac{3}{4\pi} \frac{\epsilon - 1}{\epsilon(2\epsilon + 1)} \quad (17)$$

and one arrives at the result²⁷

$$\frac{\epsilon}{\epsilon_{\text{mix}}} = 1 + \eta_0 \frac{3(\epsilon - 1)}{2\epsilon + 1}. \quad (18)$$

This equation is consistent with the Maxwell-Wagner theory²⁸ in the limit of small volume fraction η_0 .

Figure 8 illustrates the application of Eq. (18) to solutions of ionic and hydrogen-bonding substances in water.²⁹⁻³¹ The closed squares in the figure show the relative dielectric constant increment $\Delta\epsilon/\epsilon$, $\Delta\epsilon = \epsilon_{\text{mix}} - \epsilon$ for hydrated lysozyme.^{29,33} At the pH of the measurements the protein carries the total charge of +10 electron units. Open circles in the figure show the results for the dioxane-water mixture.³⁰ Dioxane offers strong hydrogen-bond acceptor sites. Finally, diamonds and the dash-dotted line show, respectively, hydrated glucose³¹ and trehalose,³² both offering multiple hydrogen-bonding sites. All these solutes, potentially breaking the interfacial network of hydrogen bonds, either follow the prescription of Maxwell's electrostatics [Eq. (18), solid line]

or deviate upward from it. The latter case, of two saccharides (glucose and trehalose), is particularly curious. According to the measurements shown in Fig. 8, sugars leave a very small dielectric footprint in aqueous solutions because their response function χ_1 is more negative than for Maxwell's dielectrics.

The Lorenz interface with $\chi_1 = 0$ is indicated by the dashed line in Fig. 8. It shows a much enhanced sensitivity of the dielectric constant to non-polar impurities than the Maxwell interface shown by the solid line. A much steeper slope implies a significant free energy penalty for polarizing such mixtures. Experimental testing of such mixtures should therefore meet with obvious solubility difficulties. However, the analysis shown in Fig. 8 suggests that the concept of an effective surface charge density σ_P , capturing different realizations of the orientational dipolar order at the interface, may present a useful conceptual framework for developing theories of polar response not restricted by Maxwell's boundary conditions.

While uniform fields of the dielectric experiment measure the dipolar response of the entire solution, non-uniform external fields give access to the response function χ_1 and therefore to the dipolar polarization of the interface. If the external field varies on a scale large compared to the dimension of the solute, the interfacial dipole couples to the field gradient. The result is a force acting on the solute

$$F_z = (\Omega_0/2)\chi_1\nabla_z E_{\text{ext}}(z)^2, \quad (19)$$

where the z -axis is chosen along the external field. This phenomenon, known as dielectrophoresis,³⁴ allows a direct access to the polarization of the interface. Equation (17) for χ_1 leads to the standard dielectrophoresis coefficient $K \propto \chi_1$ used in the theory of colloidal suspensions.³⁴ In these applications, ϵ is typically replaced with the ratio of the dielectric constants of the solvent and the solute, $\epsilon \rightarrow \epsilon/\epsilon_0$, with the result

$$K = \frac{\epsilon_0 - \epsilon}{\epsilon_0 + 2\epsilon}. \quad (20)$$

If the solute is more polar than the solvent, one gets positive dielectrophoresis ($K > 0$, $\chi_1 > 0$), and solute's attraction to a stronger electric field. The opposite case of $K < 0$ ($\chi_1 < 0$) implies negative dielectrophoresis and thus repulsion of the solute from the field.

V. SUMMARY

This paper extends our previous studies^{14,15} of dipolar fluids interfacing hard-sphere cavities to attractive non-polar solutes hydrated by SPC/E water. In-plane orientational structure of the surface dipoles holds for interfaces of both dipolar liquids and water. The orientational distribution of the interfacial dipoles alters the boundary conditions of the polar response problem monitored here in terms of the electric field inside the solute. Like in

previous studies of cavities in dipolar fluids, the field inside the solute does not follow the prediction of Maxwell’s electrostatics [Eq. (1)] and instead tends, with increasing solute size, to the limit established by the Lorentz field of a non-polarized interface [Eq. (2)].

We find that the deviation of the cavity field from the Lorentz result is given by the dipolar response function of the interface that also enters the dielectric constant of an ideal solution. Finding the slope of the dielectric increment of the low-concentration mixture vs the solute concentration [Eq. (16)] thus provides a direct input into the cavity field [Eq. (13)]. This statement also applies to the frequency-dependent response and can be used to find the refractive index corrections for rates of radiative decay of photoexcited chromophores³⁵ and quantum dots³⁶ in solution. According to our present result, this input should be sought from measuring the refractive index of corresponding mixtures.

We also find that small differences in the cavity field, which are hard to resolve within the current simulation protocol, propagate in very substantial differences in the dielectric response of a mixture. While this fact also spells out a thermodynamic difficulty of preparing solutions that might test the Lorentz interface by conventional dielectric spectroscopy, a large difference in the slopes of dashed (Lorentz) and solid (Maxwell) lines in Fig. 8 leaves much space to looking for intermediate scenarios.

Returning to the question posed in the Introduction, the liquid interface assumes the structure that makes its contribution to the field inside and outside the solute essentially null. The whole solvent response to an external polarizing field is given by the uniform polarization of the bulk and does not include an inhomogeneous component due to the surface charge [second summand in Eq. (12)]. In retrospect, this outcome should have been expected. The standard practice of liquid state theories and corresponding numerical simulations suggests a short propagation length of perturbations in liquids. A cavity or a non-polar solute should therefore be “invisible” to an observable (e.g., Maxwell field) measured a few solvent diameters from the interface, as indeed our results show. This result of course goes against the concept of the surface charge inducing a long-ranged Coulomb perturbation in the solvent.

The original concept of electric polarization envisioned by Maxwell anticipates a limited, elastic response of medium’s electric charge to an external electric field.³ For molecular dipoles of a dielectric material, this concept implies limited small-amplitude reorientations of the dipoles, aligning them with a weak external field (linear response). This physical picture, which seems to match the problem of dipolar polarization of a free solid-like interface, was historically extended to liquid dielectrics which, in contrast, have more extended ability to respond by both changing the positions of their dipoles and producing large-amplitude dipolar reorientations. In other words, the translational and rotational mobility

supported by the liquid phase allows the surface dipoles to react to the creation of the interface by rearranging their dipolar orientations in a way of diminishing the stress of a sharply varying density profile. This orientational order responds to a weak external field by the rules that do not require a surface charge and the induction of an interfacial dipole combining the negative and positive lobes of the surface charge density (Fig. 1a). The boundary conditions applicable to these systems differ from the ones anticipated for Maxwell dielectrics.

By the way of yet another historical aberration, the standard theory of dielectrics has been mostly applied not to free liquid interfaces, for which Maxwell’s construct was put forward, but to highly hydrophilic and wetted interfaces covered with surface ions or to solvation of molecular ions (Born theory of ion solvation and its extensions). The agreement between observations done for these surfaces and solutions with the predictions of dielectric models is often used to support the conceptual framework of dielectric theories developed for free or non-wetted (small attraction) surfaces. Our present development cautions against this inconsistency and points out that the orientational structure of the interface defines boundary conditions of dielectric theories and with that the microscopic and macroscopic fields observed near dielectric interfaces.

The picture of in-plane dipolar polarization of the liquid interface is rather robust and insensitive to the interface curvature. It holds even for planar surfaces (filled diamond in Fig. 5)^{9,37} suggesting that the conclusions reached here for an admittedly narrow range of solute radii may extend to larger solutes of potentially meso-to-macroscopic size.

What matters for the boundary conditions entering the electrostatic response functions is the orientational distribution of surface waters. This can be altered by surface ions and polar groups^{12,38–40} which potentially can create a non-zero surface charge density $\sigma_P \neq 0$ matching the standard conditions of Maxwell’s electrostatics. The standard prescriptions will apply to those cases. It follows directly from Coulomb’s law that the change of the normal component of the electric field at the interface of a dielectric with vacuum is related to the surface charge density, $-\Delta E_n = 4\pi\sigma_P$. The near-zero σ_P then implies the continuation of the normal component of the electric field, and, therefore, the continuation of the vector \mathbf{E} of the Maxwell field across a dielectric interface.

Liquids with large cohesive energy, network liquids, such as water, in particular, seem to be particularly relevant to this discussion. The strength of hydrogen bonds ($\sim 4 - 5 k_B T$ per bond¹⁸) is so significant that in-plane dipolar pattern may withstand local electric fields of solute partial charges. The ratio of the characteristic strengths of the solute-solvent to solvent-solvent interactions will therefore determine the orientational distribution of the surface dipoles and, ultimately, the type of boundary conditions used in calculations of the electrostatic response.

ACKNOWLEDGMENTS

This research was supported by the National Science Foundation (CHE-0910905). CPU time was provided by the National Science Foundation through TeraGrid resources (TG-MCB080116N). We are grateful to Peter Rossky for useful discussions and comments on the manuscript.

REFERENCES

- ¹L. D. Landau and E. M. Lifshitz, *Electrodynamics of continuous media* (Pergamon, Oxford, 1984).
- ²W. Thompson Lord Kelvin, *Reprint of Papers on Electrostatics and Magnetism*, 2nd ed. (MacMillan and Co., London, 1884, sec 479).
- ³J. C. Maxwell, *A Treatise on Electricity and Magnetism*, Vol. 2 (Dover Publications, New York, 1954, secs. 395-400).
- ⁴C. J. F. Böttcher, *Theory of Electric Polarization*, Vol. 1 (Elsevier, Amsterdam, 1973).
- ⁵B. W. Ninham and P. Lo Nostro, *Molecular Forces and Self Assembly In Colloids, Nano Sciences, and Biology* (Cambridge University Press, Cambridge, 2010).
- ⁶C. Y. Lee, J. A. McCammon, and P. J. Rossky, *J. Chem. Phys.* **80**, 4448 (1984).
- ⁷S. H. Lee, J. C. Rasaiah, and J. B. Hubbard, *J. Chem. Phys.* **85**, 5232 (1986).
- ⁸J. P. Valleau and A. A. Gardner, *J. Chem. Phys.* **86**, 4162 (1987).
- ⁹V. P. Sokhan and D. J. Tildesley, *Mol. Phys.* **92**, 625 (1997).
- ¹⁰D. Bratko, C. D. Daub, and A. Luzar, *Faraday Disc.* **141**, 55 (2009).
- ¹¹P. J. Rossky, *Farad. Disc.* **146**, 13 (2010).
- ¹²S. Romero-Vargas Castrillón, N. Giovambattista, I. A. Aksay, and P. G. Debenedetti, *J. Phys. Chem. C* **115**, 4624 (2011).
- ¹³L. R. Pratt, G. Hummer, and A. E. Garcia, *Biophys. Chem.* **51**, 147 (1994).
- ¹⁴D. R. Martin and D. V. Matyushov, *Europhys. Lett.* **82**, 16003 (2008).
- ¹⁵D. R. Martin and D. V. Matyushov, *J. Chem. Phys.* **129**, 174508 (2008).
- ¹⁶The concept of surface charge density is used in Ref. 4 to calculate the Lorentz field. While the procedure yields the correct algebraic result, the usage of this concept for a virtual surface is incorrect and should be avoided.
- ¹⁷G.M.Torrie and G. N. Patey, *J. Phys. Chem.* **97**, 12909 (1993).
- ¹⁸D. van der Spoel, P. J. van Maaren, P. Larsson, and N. Timneanu, *J. Phys. Chem. B* **110**, 4393 (2006).
- ¹⁹See supplementary material at [URL will be inserted by AIP] for details of the simulation protocol.
- ²⁰G. Hummer and S. Garde, *Phys. Rev. Lett.* **80**, 4193 (1998).
- ²¹I. Brovchenko and A. Oleinikova, *Interfacial and confined water* (Elsevier, Amsterdam, 2008).
- ²²D. R. Martin and D. V. Matyushov, *Phys. Rev. E* **78**, 041206 (2008).
- ²³K. A. Sharp and J. M. Vanderkooi, *Acc. Chem. Res.* **43**, 231 (2010).
- ²⁴Y. R. Shen, *Solid State Comm.* **108**, 399 (1998).
- ²⁵H. S. Ashbaugh, *J. Phys. Chem. B* **104**, 7235 (2000).
- ²⁶A. D. Friesen and D. V. Matyushov, *Chem. Phys. Lett.*, 10.1016/j.cplett.2011.06.031(2011).
- ²⁷D. V. Matyushov, *Phys. Rev. E* **81**, 021914 (2010).
- ²⁸B. K. P. Scaife, *Principles of dielectrics* (Clarendon Press, Oxford, 1998).
- ²⁹C. Cametti, S. Marchetti, C. M. C. Gambi, and G. Onori, *J. Phys. Chem. B* **115**, 7144 (2011).
- ³⁰S. Schrödle, G. Hefter, and R. Buchner, *J. Phys. Chem. B* **111**, 5946 (2007).
- ³¹H. Weingärtner, A. Knocks, S. Boresch, P. Hocht, and O. Steinhauser, *J. Chem. Phys.* **115**, 1463 (2001).
- ³²W. M. Arnold, A. G. Gessner, and U. Zimmermann, *Biochim. Biophys. Acta* **1157**, 32 (1993).
- ³³The analysis of the dielectric constant of the lysozyme solution neglects the dipole moment of the protein. Its contribution requires special consideration since it involves not only the variance of the protein dipole itself, but also the cross-correlation between the dipoles of the protein and hydration layer.
- ³⁴T. B. Jones, *Electromechanics of Particles* (Cambridge University Press, Cambridge, 1995).
- ³⁵D. Topygin, *J. Fluoresc.* **13**, 201 (2003).
- ³⁶S. F. Wuister, C. D. Donega, and A. Meijerink, *J. Chem. Phys.* **121**, 4310 (2004).
- ³⁷Y. R. Shen and V. Ostroverkhov, *Chem. Rev.* **106**, 1140 (2006).
- ³⁸A. Verdaguer, G. M. Sacha, H. Bluhm, and M. Salmeron, *Chem. Rev.* **106**, 1478 (2006).
- ³⁹A. L. Barnette, D. B. Asay, and S. H. Kim, *Phys. Chem. Chem. Phys.* **10**, 4981 (2008).
- ⁴⁰K. C. Jena and D. K. Hore, *Phys. Chem. Chem. Phys.* **12**, 14383 (2010).